# Supplementary Information

# ‘Cable Bacteria Control Iron-Phosphorus Dynamics in Sediments of a Coastal Hypoxic Basin’

Fatimah Sulu-Gambari[1*], Dorina Seitaj[2], Filip J. R. Meysman[2], Regina Schauer[3], Lubos Polerecky[1], Caroline P. Slomp[1]

[1] Department of Earth Sciences (Geochemistry), Faculty of Geosciences, Utrecht University, Utrecht, the Netherlands

[2] Department of Ecosystem Studies, Royal Netherlands Institute for Sea Research, Yerseke, the Netherlands

[3] Center for Geomicrobiology and Section for Microbiology, Department of Bioscience, Aarhus University, Aarhus, Denmark

## 1.1. Monthly Changes in Pore water Sulfate: Impact of Cable Bacteria

Pore water depth-profiles of sulfate for January to June 2012 clearly deviate from those recorded for August to December 2012 (Figure S1). The latter set of profiles show the typical decline with depth that is expected for non-bioturbated sediments, i.e. the concave curvature that results from sulfate consumption due to sulfate reduction. The sulfate depth-profiles for January to June 2012 however, either show a convex shape indicative of sulfate production in the upper 4 cm (January, March, June), or a near-linear decline with depth (February, April, May) in some cases, followed by a concave shape in line with sulfate consumption in deeper sediment layers (January, April, June). This characteristic sulfate pore water profile has been linked to the activity of cable bacteria, based on laboratory experiments[1] and model simulations[2], where the production of sulfate in the top sediment layer results from the

dissolution and oxidation of iron sulfides promoted by the strong acidification of the pore water by cable bacteria activity. The signals for cable bacteria are most clearly developed in January and March.

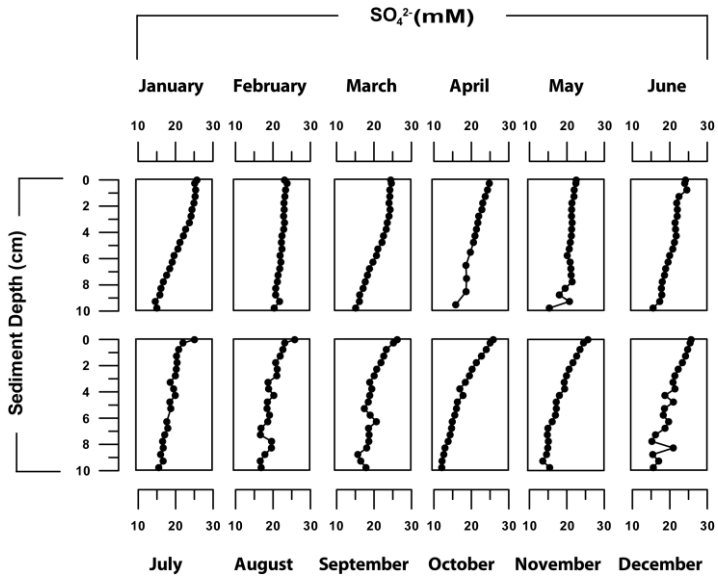


**Figure S1:** Seasonal variation in the profiles for sulfate in Lake Grevelingen sediments.

## 1.2.Seasonal Variation in Solid-Phase Manganese

Solid-phase Mn is abundantly present in the surface sediment in spring, but is absent in summer and fall (Figure S2).

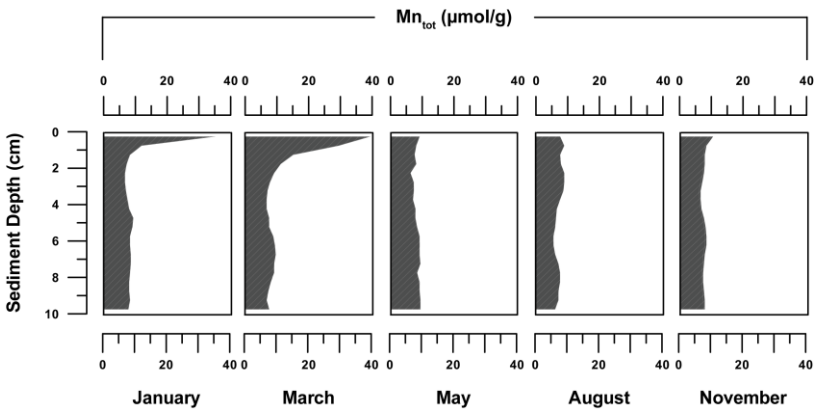


**Figure S2:** Depth-profiles of total manganese in the sediment for January, March, May, August and November 2012, highlighting strong seasonal variation.

## 1.3.Seasonality in Sediment Phosphorus Forms and Fe sulfide

Depth-profiles of exchangeable P and Fe-oxide bound P in March differ greatly from those in November in 2012, but there is little change in authigenic P, detrital and organic P (Figure S3).

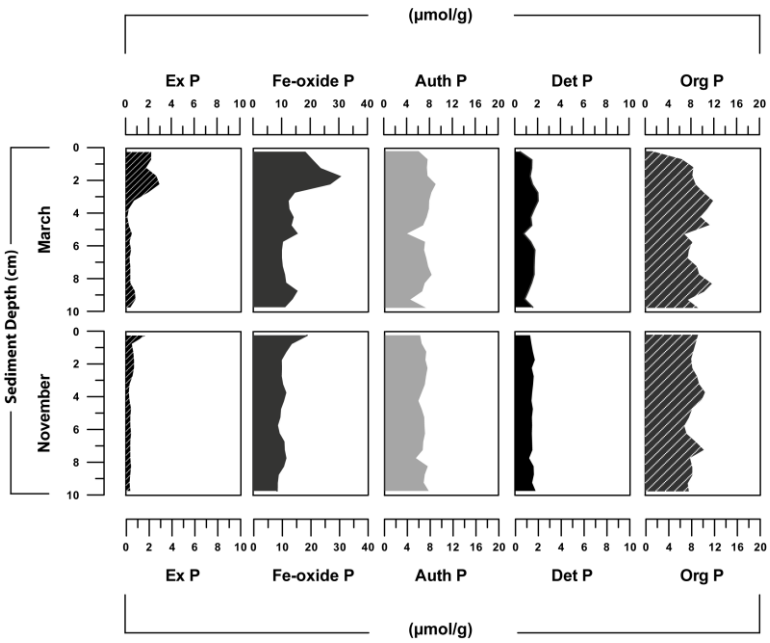


**Figure S3:** Sediment P forms (in µmol/g) in March and November 2012.

There is substantial seasonal variation in Fe-oxide bound P and FeS in Grevelingen sediments from January to November 2012, where Fe-oxide-bound P is enriched in FeS-poor sediments in spring (Figure S4). The zone of FeS dissolution extends down to a depth of 2 to 4 cm in spring (Figure S4), despite a very shallow penetration depth of oxygen throughout the year (at most ~3mm; see Figure 1, Seitaj *et al*.[6]).

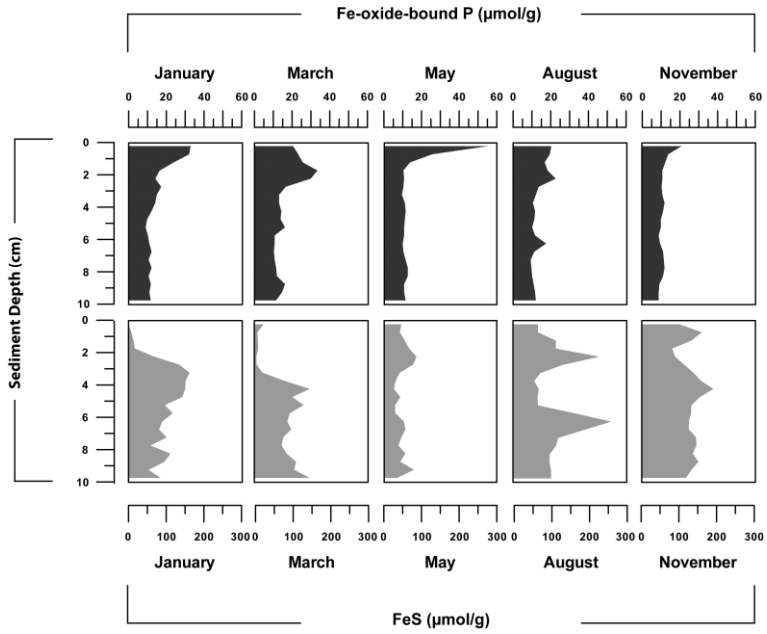


**Figure S4:** Depth profiles of sediment Fe-P and FeS for January, March, May, August and November 2012.

## 1.4. Oxidants for $Fe^{2+}$

Ferrous iron ($Fe^{2+}$) can be oxidized below the oxic zone with either nitrate[3] or manganese oxide[4] as an oxidant, following:

$$10Fe^{2+} + 2NO_3^- + 24H_2O \rightarrow 10Fe(OH)_3 + N_2 + 8H^+ \qquad (S1)$$

$$2Fe^{2+} + MnO_2 + 2H_2O + 2H^+ \rightarrow 2Fe(OH)_3 + Mn^{2+} \qquad (S2)$$

All pore water $Fe^{2+}$ was removed above 1.25 cm depth in March. Diffusive fluxes of $Fe^{2+}$ and nitrate to the removal zone were calculated using diffusion coefficients taken from Boudreau[5], corrected for the ambient temperature, salinity and porosity. The diffusive $Fe^{2+}$ flux was estimated from the pore water gradient in $Fe^{2+}$ (Figure 2) at 4 mmol $m^{-2}$ $d^{-1}$. Using the bottom-water nitrate concentration of 30 µM, and assuming the supply of nitrate through nitrification in this zone to be negligible, the maximum nitrate flux to this zone was estimated at ca. 0.22 mmol $m^{-2}$ $d^{-1}$. Given the 5:1 stoichiometry of the reaction between $Fe^{2+}$ and $NO_3^-$, this implies that at most 27% of the dissolved $Fe^{2+}$ could be oxidized with nitrate. Manganese

oxides are abundantly present in the surface sediment in March (Figures 2 and S2) and concentrations of $Mn^{2+}$ rise with depth where $Fe^{2+}$ is removed. Concentrations of both solutes are of the same order of magnitude. Given the 2:1 stoichiometry of the reaction between $Fe^{2+}$ and $MnO_2$, this implies that sufficient Manganese oxides were present to explain the oxidation of $Fe^{2+}$.

**1.5. Fe-oxide data**

Sedimentary Fe fractions were determined using the method of Poulton and Canfield[7], where Fe-oxides were estimated as the total of the non-sulphidized Fe pools extracted with a 1 M hydroxylamine-HCl solution in 25% v/v acetic acid and sodium dithionite solution (50 g $L^{-1}$), buffered to pH 4.8. The contents of Fe-oxides were corrected for FeS dissolution, by subtracting the measured sulfide concentration for each sediment interval, determined as Acid Volatile Sulfide (AVS) from the S extractions. Measured Fe concentrations from duplicate analyses varied less than 5%.

There is a buildup of Fe-oxides in the surface sediments between January and March (Figure S5). From May onwards, the Fe oxides start to be removed, although an enrichment near the sediment-water interface is still visible. Low concentrations are observed in November (Figure S5). Changes in background values of Fe-oxides likely reflect spatial variations in the contribution of more refractory Fe-oxides.

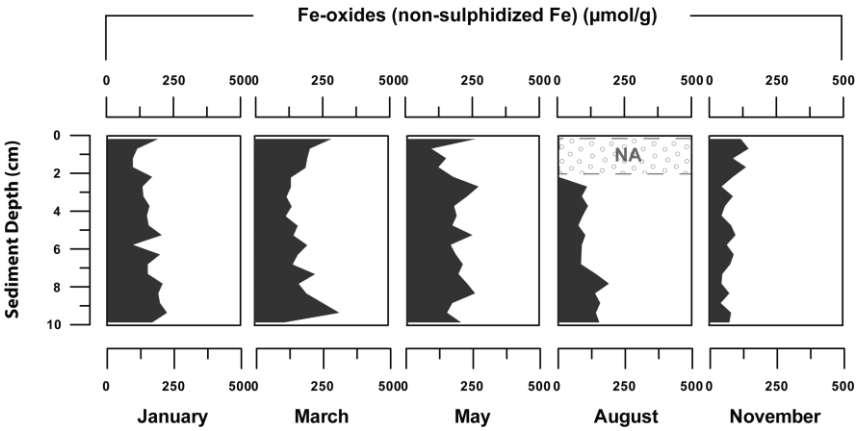


**Figure S5:** Depth profiles of sediment Fe-oxides for January, March, May, August and November 2012.

## 1.6. Impact of cable bacteria on sedimentary P cycling at a second site in the basin

Data from an additional site (17m) in Lake Grevelingen demonstrate a direct link between seasonal changes in cable bacteria abundance and sedimentary P-dynamics. This shallower location is subject to a significantly lower sedimentation rate (~0.4 cm/yr) than the deeper site. In both spring and fall of 2012, a suboxic zone devoid of oxygen and free sulfide developed in the surface sediment at depths down to 26.1 mm and 18.2 mm respectively.

Microscopic examination of the sediment using fluorescence in situ hybridization (FISH; probe DSB 706) revealed a high abundance of cable bacteria in March and May down to a depth of 40 mm and micro-sensor depth-profiles of $O_2$, $\Sigma H_2S$ and pH showed the characteristic geochemical signature of electrogenic sulfur oxidation[1, 2] (Figure S6). Similar to the deeper site, cable bacteria were undetected with the onset of hypoxia and from September onwards, Beggiatoaceae were present at the sediment surface.

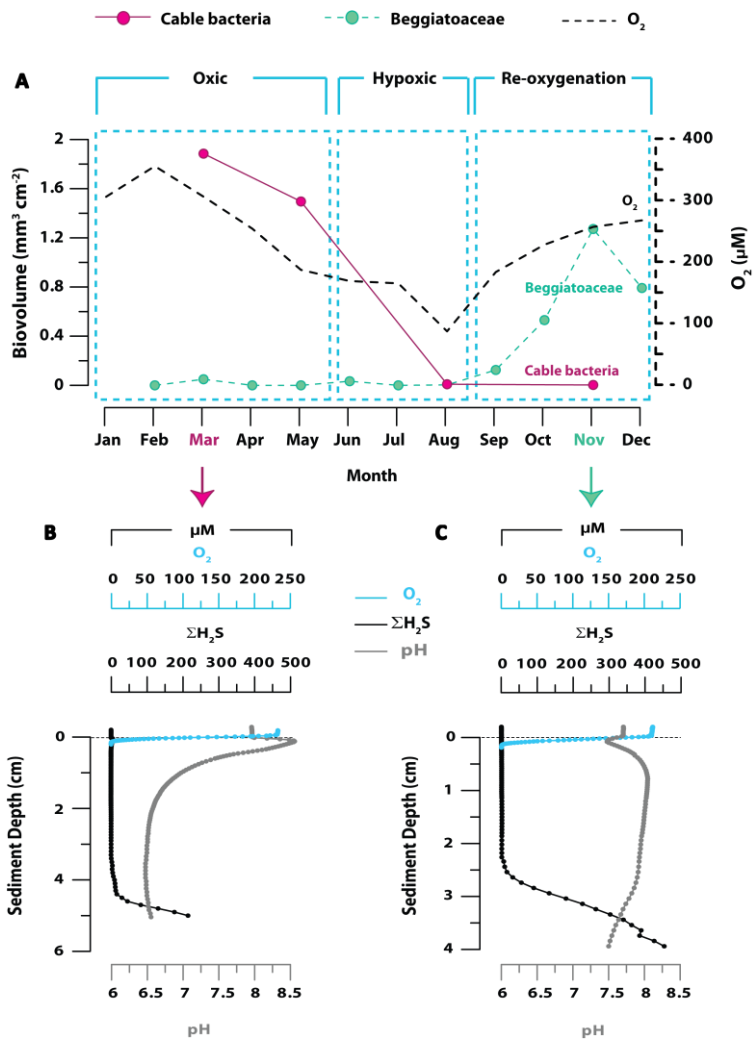


**Figure S6:** (A) Temporal changes in oxygen concentrations in the bottom water and bacterial succession at the sediment surface at an additional site (17m) in 2012. The abundance of cable bacteria filaments (pink dots) was determined in March, May, August and November only, whereas for Beggiatoaceae (green dots) data were obtained for each sampling month. Micro-sensor profiles of oxygen, hydrogen sulfide and pH in sediment pore water in March (B) and November (C) for the site at 17m-depth. Cable bacteria fingerprints are characterized by a broad subsurface pH-minimum while Beggiatoaceae create a broad pH-maximum in the suboxic zone, reflecting the effect of bacterial succession on sediment pore water chemistry at this site, as both types of bacteria induce the formation of oxygen- and sulfide-free suboxic zones.

In March there is production of $Fe^{2+}$, $Mn^{2+}$, $Ca^{2+}$ and $SO_4^{2-}$ in the pore water, accompanied by evidence for the removal of $PO_4$ from the pore water just above this sedimentary horizon in

spring (Figure S7a). Later on in the year, the sediment pore water profiles are characterized by trends with depth that are typical for hypoxic sediments (Figure S7a).

Total P and total Mn are strongly enriched in the surface sediment in spring, a feature which is absent in November (Figure S7b). In March, sediment concentrations of total sulfur (Stot) decrease towards the sediment-water interface, consistent with dissolution of Fe-sulfides in the suboxic zone. In November, under more reducing sediment conditions and in the absence of cable bacteria, sulfur in the surface sediment is replenished (Figure S7b).

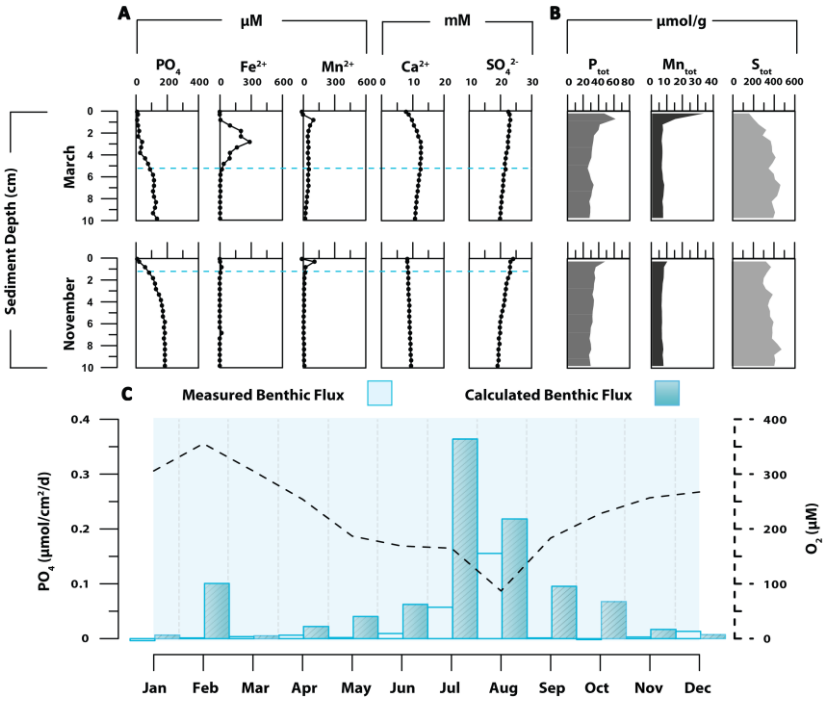


**Figure S7:** Geochemical imprint of cable bacteria at an additional site (17m). (A) Pore water [$PO_4$], [$Fe^{2+}$], [$Mn^{2+}$], [$Ca^{2+}$] and [$SO_4^{2-}$] for March 2012, when cable bacteria are present and November 2012, when Beggiatoaceae are abundant in the sediment. Dashed lines indicate the depths below which hydrogen sulfide is detectable. (B) Solid-phase total P ($P_{tot}$), total Mn ($Mn_{tot}$), and total S ($S_{tot}$) for March and November 2012. (C) Flux of phosphate from the sediment to the water column as measured in incubations and calculated from pore water profiles from cores collected at 17m (in µmol $cm^{-2}$ $d^{-1}$).

Similar to the deep site, there is generally little release of phosphate from the sediment to the overlying water in spring (Figure S7c). From late spring onwards, the decline in bottom-water oxygen during seasonal stratification coincides with increased release of phosphate from the sediment (Figure S7c).

Bottom-water $PO_4$ and $O_2$ concentrations for 2012 and 2013 in the basin show similar seasonal trends, with low concentrations of $PO_4$ in the oxygenated bottom water in spring and elevated concentrations of $PO_4$ in summer following the onset of hypoxia (Table S1). The larger amplitude of the seasonal change in $PO_4$ concentrations in 2013 is likely the direct consequence of the lower bottom-water oxygen concentrations in that year. The low bottom-water $PO_4$ concentrations in spring of 2013 are consistent with retention of $PO_4$ in the sediment due to activity of the cable bacteria.

| | 2012 | | 2013 | |
|---|---|---|---|---|
| **Bottom-water conc. (µM)** | **$O_2$** | **$PO_4$** | **$O_2$** | **$PO_4$** |
| **Jan** | 247.82 | 1.12 | 260.63 | 1.18 |
| **Feb** | 300.64 | 0.95 | 296.88 | 1.02 |
| **Mar** | 309.07 | 0.49 | 253.13 | 1.09 |
| **Apr** | 239.07 | 0.44 | 303.07 | 0.15 |
| **May** | 153.13 | 1.67 | 188.90 | 1.89 |
| **Jun** | 72.50 | 4.51 | 84.27 | 3.33 |
| **Jul** | 40.63 | 5.83 | 0.00 | 7.40 |
| **Aug** | 3.44 | 6.82 | 0.00 | 10.80 |
| **Sep** | 190.56 | 1.77 | 0.00 | 11.10 |
| **Oct** | 239.07 | 1.54 | 213.67 | 1.30 |
| **Nov** | 237.54 | 1.51 | 225.59 | 1.76 |
| **Dec** | 259.98 | 1.32 | 159.69 | 2.73 |

**Table S1:** Temporal changes in oxygen and phosphate concentrations (µM) in the bottom-water in 2012 and 2013.

### 1.7. Benthic Flux Calculations

Diffusive fluxes of phosphate across the sediment-water interface were calculated from the pore water depth-profiles, as the phosphate concentration gradient between bottom water and

topmost pore water value (Figure S8). Fluxes were determined using diffusion coefficients taken from Boudreau[5], corrected for the ambient temperature, salinity and porosity.

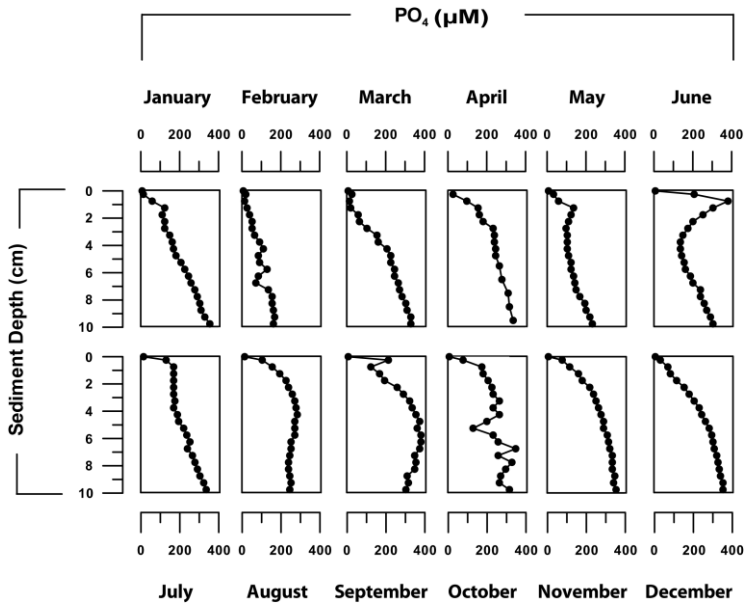


**Figure S8:** Profiles of pore water phosphate for each Month in 2012, highlighting a strong seasonality in the retention and release of phosphate in the sediment.

## 1.8. Polyphosphate in Cable Bacteria

Intracellular phosphorus (P) content in individual cells of cable bacteria was estimated using nanometer-scale secondary ion mass spectrometry (NanoSIMS). The analysis was performed as previously described by Vasquez-Cardenas *et al*. (2014)[8] using a NanoSIMS 50L instrument (Cameca, France) at Utrecht University and the data processing freeware programme, Look@NanoSIMS[9]. Two sediment cores with abundant cable bacteria were incubated with $^{13}$C-labeled bicarbonate and propionate. Individual filaments were then hand-picked from the oxic (0-0.2cm depth) and suboxic zones (0.4-2.0 cm depth) and analysed for counts of secondary ions $^{12}C^-$, $^{13}C^-$, and $^{31}P^-$, which were subsequently used to calculate the P/C ratio as $\frac{^{31}P}{(^{12}C + {}^{13}C)}$. Overall, three to eight different filaments were analysed from each treatment and zone. Only active cells were used in the analysis, where the activity was

determined based on their $^{13}C$-enrichment in comparison to the control cells (see Vasquez-Cardenas *et al*.[10]).

NanoSIMS images revealed that active cable bacteria contained clear P-rich inclusions (exemplary cells from the suboxic zone of the $^{13}C$-proprionate incubation core are shown in Figure 3a). Based on a total of 87 individual cells and 70 P inclusions (Figure S9), we determined that the P/C ratio in inclusions was on average 5.6-fold greater than that of the rest of the cell, and that the area of an inclusion comprised on average 4.2% of the total planar cell area in the nanoSIMS image.

It is known that due to differences in ionisation behaviour of different elements the sensitivity of nanoSIMS generally varies depending on the element and the matrix from which they are mobilised by the primary ion beam. Thus, to calibrate the semi-quantitative nanoSIMS data we assumed that the average P/C ratio determined by nanoSIMS for the cell *without* inclusions (0.022; see red symbols in Figure S2) was equal to the Redfield ratio $\left(\frac{1}{106}\right)$. To make the estimation of the P/C ratio in active cells of the cable bacteria possible, we additionally assumed that this calibration was matrix-independent, i.e., the same when detecting C and P from the material comprising the cell and from the material comprising the P-rich inclusions. Taking into account that there were 2 inclusions on average per cell (e.g. Figure 3a), these assumptions led to the estimated average P/C ratio of the individual cable bacteria cell of $(1 - 2 \times 0.042) \times \frac{1}{106} + 2 \times 0.042 \times \frac{5.6}{106} = 0.0131$, which is about 38% larger than the Redfield ratio.

The cable bacteria biovolume was highest in March 2012 at 2.3 $mm^3$ $cm^{-2}$. Using the empirical equation of Loferer-Krossbacher *et al*.[11] (dw = 4.35 x $V^{0.86}$, where the dry weight,

dw, is calculated in fg and the volume, V, is in µm3) and assuming a cellular carbon content of 50%[12], the cable bacteria biomass was estimated at 20 mmol C $m^{-2}$. Using the P/C ratio estimated above, this translates to a P-content of about 0.3 mmol P $m^{-2}$. Thus the intracellular P-content of active cable bacteria is negligible in comparison to the change in the Fe-P inventory observed from May to August (47.9 mmol P $m^{-2}$). Note that this conclusion would hold even if the P/C ratio in cable bacteria estimated by nanoSIMS was grossly underestimated. For example, even if the P/C ratio was 10-fold larger than the Redfield ratio, the sedimentary P content due to cable bacteria would amount to about 1.9 mmol P $m^{-2}$ and would therefore still be unable to explain the observed change in the Fe-P inventory.

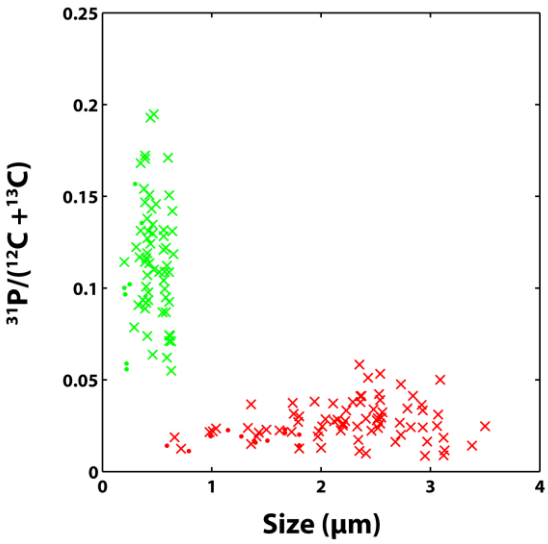


**Figure S9:** NanoSIMS analysis of P/C ratios for individual cable bacteria cells. Shown are P/C ratios, calculated from the measured secondary-ion counts, versus size (in µm) determined for P-rich inclusions (green) and cells without inclusions (red). Dots and crosses correspond to cells incubated with $^{13}$C-bicarbonate and $^{13}$C-propionate, respectively.

### 1.9. Impact of Beggiatoaceae on sedimentary P cycling

The release of large amounts of intracellular phosphate from sulfur-oxidizing bacteria such as *Thiomargarita* and *Beggiatoa* can result in formation of apatite in sediments[13] and may

impact benthic exchange[14]. Concentrations of authigenic apatite show little change with depth in the sediment (Figure S3) and are comparable to concentrations in suspended matter (e.g., 6.0 and 6.2 µmol/g for March and November, respectively). Moreover, there is no evidence for a significant impact on pore water profiles of phosphate during months that Beggiatoaceae are most abundant (October to December) (Figure 1). This suggests that Beggiatoaceae are not significantly impacting sediment-water exchange of P nor are inducing apatite formation in these sediments to a significant extent, confirming earlier suggestions that the reported effect of sulfide-oxidizing bacteria on apatite formation[13, 15] is not ubiquitous in hypoxic marine sediments[16].

## 1.10. Measured Benthic Fluxes

**Table S2:** Flux of phosphate from the sediment to the water column as measured in incubations in cores collected at 34 and 17m (in µmol $cm^{-2}$ $d^{-1}$).

| | Site 1 | | | | | Site 3 | | | | |
|---|---|---|---|---|---|---|---|---|---|---|
| **Measured benthic flux (µmol $cm^{-2}$ $d^{-1}$)** | **Core 1** | **Core 2** | **Core 3** | **Av.** | **St.Dev** | **Core 1** | **Core 2** | **Core 3** | **Av.** | **St.Dev** |
| **Jan** | 0.003 | 0.004 | | 0.004 | 0.001 | -0.005 | -0.003 | | -0.004 | 0.002 |
| **Feb** | 0.005 | 0.002 | | 0.003 | 0.003 | 0.001 | 0.002 | | 0.001 | 0.000 |
| **Mar** | 0.014 | 0.008 | 0.013 | 0.012 | 0.004 | 0.003 | 0.004 | 0.004 | 0.004 | 0.000 |
| **Apr** | 0.010 | 0.012 | | 0.011 | 0.001 | 0.006 | 0.006 | | 0.006 | 0.000 |
| **May** | 0.387 | 0.198 | | 0.292 | 0.133 | 0.005 | 0.000 | | 0.002 | 0.003 |
| **Jun** | 0.170 | 0.342 | | 0.256 | 0.121 | 0.011 | 0.007 | | 0.009 | 0.003 |
| **Jul** | 0.146 | 0.226 | | 0.186 | 0.057 | 0.051 | 0.064 | | 0.057 | 0.009 |
| **Aug** | 0.288 | 0.444 | 0.299 | 0.344 | 0.087 | 0.174 | -0.076 | 0.197 | 0.099 | 0.151 |
| **Sept** | 0.166 | 0.086 | | 0.126 | 0.057 | 0.015 | -0.013 | | 0.001 | 0.020 |
| **Oct** | 0.050 | 0.058 | | 0.054 | 0.005 | -0.002 | -0.002 | | -0.002 | 0.000 |
| **Nov** | 0.039 | 0.036 | 0.211 | 0.095 | 0.100 | 0.003 | 0.001 | 0.005 | 0.003 | 0.002 |
| **Dec** | -0.011 | 0.011 | | 0.000 | 0.015 | 0.010 | 0.017 | | 0.013 | 0.005 |

## References


1. Risgaard-Petersen, N.; Revil, A.; Meister, P.; Nielsen, L. P., Sulfur, iron-, and calcium cycling associated with natural electric currents running through marine sediment. *Geochimica et Cosmochimica acta* **2012,** *92*, (0), 1-13.
2. Meysman, F. J. R.; Risgaard-Petersen, N.; Malkin, S. Y.; Nielsen, L. P., The geochemical fingerprint of microbial long-distance electron transport in the seafloor. *Geochimica et Cosmochimica Acta* **2015,** *152*, (0), 122-142.

3. Straub, K. L.; Benz, M.; Schink, B.; Widdel, F., Anaerobic, nitrate-dependent microbial oxidation of ferrous iron. *Applied and environmental microbiology* **1996,** *62*, (4), 1458-60.
4. Reed, D. C.; Slomp, C. P.; Gustafsson, B. G., Sedimentary phosphorus dynamics and the evolution of bottom water hypoxia: A coupled benthic-pelagic model of a coastal system. *Limnology and Oceanography* **2011,** *56*, (1075-1092).
5. Boudreau, B. P., *Diagenetic Models and their Implementation*. Springer: 1997; p 430.
6. Seitaj, D.; Schauer, R.; Sulu-Gambari, F.; Hidalgo-Martinez, S.; Malkin, S. Y.; Burdorf, L. D. W.; Slomp, C. P.; Meysman, F. J. R., Cable bacteria generate a firewall against euxinia in seasonally hypoxic basins. *Proceedings of the National Academy of Sciences* **2015,** *112*, (43), 13278-13283.
7. Poulton, S. W.; Canfield, D. E., Development of a sequential extraction procedure for iron: implications for iron partitioning in continentally derived particulates. *Chemical Geology* **2005,** *214*, (3–4), 209-221.
8. Vasquez-Cardenas, D.; van de Vossenberg, J.; Polerecky, L.; Malkin, S. Y.; Schauer, R.; Hidalgo-Martinez, S.; Confurius, V.; Middelburg, J. J.; Meysman, F. J. R.; Boschker, H. T. S., Microbial carbon metabolism associated with electrogenic sulphur oxidation in coastal sediments. *ISME J* **2015,** *9*, (9), 1966-1978.
9. Polerecky, L.; Adam, B.; Milucka, J.; Musat, N.; Vagner, T.; Kuypers, M. M. M., Look@NanoSIMS – a tool for the analysis of nanoSIMS data in environmental microbiology. *Environmental Microbiology* **2012,** *14*, (4), 1009-1023.
10. Vasquez-Cardenas, D.; van de Vossenberg, J.; Polerecky, L.; Malkin, S. Y.; Schauer, R.; Hidalgo-Martinez, S.; Confurius, V.; Middelburg, J. J.; Meysman, F. J. R.; Boschker, H. T. S., Microbial carbon metabolism associated with electrogenic sulphur oxidation in coastal sediments. In Royal Netherlands Institute for Sea Research (NIOZ),Yerseke, Netherlands: 2014.
11. Loferer-Krossbacher, M.; Klima, J.; Psenner, R., Determination of bacterial cell dry mass by transmission electron microscopy and densitometric image analysis. *Applied and environmental microbiology* **1998,** *64*, (2), 688-94.
12. Schauer, R.; Risgaard-Petersen, N.; Kjeldsen, K. U.; Tataru Bjerg, J. J.; B Jorgensen, B.; Schramm, A.; Nielsen, L. P., Succession of cable bacteria and electric currents in marine sediment. *ISME J* **2014,** *8*, (6), 1314-1322.
13. Schulz, H. N.; Schulz, H. D., Large Sulfur Bacteria and the Formation of Phosphorite. *Science* **2005,** *307*, (5708), 416-418.
14. Dale, A. W.; Bertics, V. J.; Treude, T.; Sommer, S.; Wallmann, K., Modeling benthic–pelagic nutrient exchange processes and porewater distributions in a seasonally hypoxic sediment: evidence for massive phosphate release by Beggiatoa? *Biogeosciences* **2013,** *10*, (2), 629-651.
15. Goldhammer, T.; Bruchert, V.; Ferdelman, T. G.; Zabel, M., Microbial sequestration of phosphorus in anoxic upwelling sediments. *Nature Geosci* **2010,** *3*, (8), 557-561.
16. Mort, H.; Slomp, C. P.; Gustafsson, B. G.; Andersen, T. J., Phosphorus recycling and burial in Baltic Sea sediments with contrasting redox conditions. *Geochimica & Cosmochimica acta* **2010,** *74*, 1350-1362.